CANCER GENOMICS & PROTEOMICS *3*: 279-288 (2006)

Molecular Assessment of the Tumor Protein Microenvironment Using Imaging Mass Spectrometry

ROBERT L. CALDWELL[1,2], ADRIANA GONZALEZ[3], STACEY R. OPPENHEIMER[1], HERBERT S. SCHWARTZ[4] and RICHARD M. CAPRIOLI[1,2]

[1]Mass Spectrometry Research Center, Departments of [2]Biochemistry and [3]Pathology and [4]Vanderbilt Orthopaedic Institute, Vanderbilt University School of Medicine, Nashville, TN, U.S.A.

Abstract. *Tumor cells or other bioreactive compounds derived from the tumor can migrate beyond the tumor margin and may be significant contributing factors in tumor recurrence. Local recurrence of cancer occurs quite often, despite microscopically-confirmed negative surgical resection margins, and is likely related to the presence of abnormal, fully neoplastic or pre-neoplastic cells adjacent to the tumor that cannot be recognized by conventional light microscopy. Identification of proteins that define the molecular tumor microenvironment of the neoplastic process may become an important part of the evaluation of cancer tissue, potentially helping guide surgical resection procedures. Tissue-based matrix-assisted laser desorption ionization (MALDI) imaging mass spectrometry is a molecular analysis technology that can significantly improve the assessment of tumor microenvironment at the molecular level. In the current study, this is illustrated with the analysis of an invasive soft tissue sarcoma. Marked differences in protein distribution between tumor and immediate adjacent tissue are shown, and these differences persist far into histologically normal appearing adjacent tissue. Several of these proteins are confirmed using immunohistochemistry. This study demonstrates that tissue-based MALDI imaging mass spectrometry is ideally suited for the molecular analysis of tumor microenvironment and could potentially augment histologic interpretation of tumor margins.*

Financial support: NIH/NIGMS 5R01 GM 58008, 5R33 CA86243-03, the T.J. Martell Foundation, the Robert J. Kleberg Jr. and Helen C. Kleberg Foundation and the Vanderbilt-Ingram Comprehensive Cancer Center.

Correspondence to: Robert L. Caldwell, Ph.D., Vanderbilt Orthopaedic Institute, Medical Center East, South Tower Suite 4200, Nashville, TN 37232-8774, U.S.A. Tel: 615-936-6296, Fax: 615-322-8043, e-mail: robert.l.caldwell@vanderbilt.edu

Key Words: Imaging mass spectrometry, tumor microenvironment, field effect.

Surgical oncologists and pathologists rely on histopathological evaluation of tumor margins to assess the success of complete excision of a tumor. Retrospective studies have confirmed that the extent of tumor resection is predictive of patient outcome (1, 2). Histological assessment of tumor margins is the primary post-operative tool used to assess the surgical procedure. Incomplete removal significantly influences the likelihood of local recurrence for several cancers, including tumors of the lung (3), prostate (4), breast (5, 6), soft tissue (7, 8), bone (8) and head and neck (9). However, histological analysis may be inadequate in determining tumor-free margins. The "field effect" has long been known in histology but the molecular abnormalities comprising this field are largely unknown. Surgical resection of diseased tissue without removal of surrounding margin leads to unacceptably high rates of recurrence (10). Cells existing in the early malignant transformation phase may appear morphologically indistinguishable from genetically normal cells. Since human solid tumors undergo multiple genetic changes as they progress from a near-normal state to aggressive invasion and malignancy, some of these changes may occur in subtle, yet distinct, predictable patterns that are not readily observed under early histologic evaluation. Thus, the ability to define and assess tumor margins can be significantly augmented by a molecular assessment of the surgical specimen.

Previous studies of tumor margins based on a single protein have been reported for several types of cancers. For example, monitoring total excision of squamous-cell carcinoma of the head and neck has focused on p53 (11, 12) and eIF4E (13, 14), while other studies utilized HER2/*neu* for breast carcinoma (5), NF-κB (15) and alpha-methylacyl-CoA racemase (16) for prostate cancer, and vascular endothelial growth factor for lung cancer (17). However, a single protein may be insufficient for this purpose and groups of protein markers, collectively, may more accurately identify potentially malignant tissue areas.

We have employed imaging mass spectrometry (IMS), a technology that allows visualization of hundreds of proteins in a tissue section, for the discovery of protein signatures that would permit molecular differentiation between neoplastic and non-neoplastic regions within the tumor-stroma interface. IMS utilizes matrix-assisted laser desorption ionization mass spectrometry (MALDI MS) to generate molecular images from a tissue section (18-20). Intact tissue sections are analyzed by a discrete raster over the tissue surface using a laser beam, where each laser spot represents a 'pixel' of the final image. The raster is usually accomplished by moving the sample under a fixed position laser beam over a predetermined two-dimensional grid, generating a full mass spectrum at each grid coordinate. Software has been optimized to automate the scanning process, including fast data acquisition, online compression and image reconstruction (21). These data are output as two-dimensional intensity maps at any given mass-to-charge (m/z) value to provide specific molecular images of that tissue. To perform the analysis, the intact tissue section is coated uniformly with a thin, homogenous layer of matrix crystals. This is amenable to automation and, in fact, we have utilized an acoustic microdispensing robotic system where matrix discrete spots ($\sim$175 μm diameter) are created in an array over the area of interest (22).

Depending on the requirements of the analysis, image resolution can be chosen by adjusting the distance between the pixels. Typically, 100 laser shots are averaged at each image coordinate, providing a spectrum that displays many hundreds of signals in a molecular weight range up to 100,000 Da, although most lie below 50,000 Da. IMS has distinct advantages over traditional techniques in ascertaining protein localization because of its unique molecular specificity. Since IMS does not require an antibody or prior knowledge of potential protein targets, it is well suited for discovery studies. Localization of all tractable proteins at each coordinate in the same tissue section can be accomplished because tissue homogenization is not required.

The purpose of this study was to assess the usefulness of tissue-based imaging mass spectrometry technology to determine protein distributions that may extend from tumor into histologically normal appearing tissue. For the case of an invasive soft tissue sarcoma used in this study, a number of proteins that traverse these regions, or that localize specifically to normal appearing tissue regions, was found. Although it will require a significant amount of additional research to define signatures for each type of cancer, this study demonstrates the effectiveness of this technology to assess molecular changes in tumor microenvironment on a molecular level. We believe this technology will be essential for the discovery of protein signatures that may augment interpretation of tumor margins and better define the biological relationship between the tumor and adjacent tissue.

Materials and Methods

Sample procurement and preparation. A high grade, recurrent malignant fibrous histiocytoma adjacent to skeletal muscle was resected from the right leg of a consenting patient and interpreted by a surgical pathologist to determine clear surgical margins. After procurement of the specimen, a representative section of tumor-margin interface was transferred to the laboratory for research purposes. The tissue section was wrapped in aluminum foil, snap-frozen in liquid nitrogen and maintained at –80˚C until further use. Prior to analysis, the tissue was cut in a cryostat in 12 μm sections and transferred to indium-tin oxide (ITO)-coated glass slides compatible for MALDI analysis (Delta Technologies Ltd.; Stillwater, MN, USA). To control for any protein delocalization that might be induced by tissue sectioning in the cryostat, sections were also cut in a reversed manner and imaged. After drying in a desiccator for 30 min, the tissue section was stained with a MALDI-compatible histological dye (Cresyl violet) as described earlier (23). A sequential section was also stained with H&E. Both tissue sections were re-examined by a surgical pathologist to confirm absence of the cancer phenotype. Microdroplets of matrix (sinapinic acid at 20 mg/mL in a mixture of 50:50:0.1 acetonitrile/H_2O/trifluoroacetic acid by volume) were microdeposited on the Cresyl violet stained tissue with a robot (Labcyte, Inc., Sunnyvale, CA, USA). Thirty rows and 100 columns of matrix with 250 μm center to center spacing between matrix spots were deposited across the entire length of the tissue section. The tissue section was then allowed to dry in a desiccator for 30 min before data acquisition.

Tissue imaging. MALDI mass spectra were acquired on a Voyager DE-STR mass spectrometer (Applied Biosystems, Foster City, CA, USA) equipped with a nitrogen laser (337 nm) with a repetition rate at 20 Hz. Data were acquired in the linear geometry mode under delayed extraction conditions with an accelerating voltage of 25 kV, 86% grid voltage, a delay time of 150 nanoseconds, and a flight path length of 2.0 m. These delayed extraction parameter coordinates allowed maximum resolution in the m/z 15,000 range. For image reconstruction, an array of coordinates was imported into the Voyager Sequence Editor software which was used for automated acquisition of spectra at each matrix spot. Spectra were baseline corrected and visualized with Biomap software (Novartis International AG; Basel, Switzerland). For constructing 3-dimensional images, Image-Pro Plus (Media Cybernetics, Inc., Silver Spring, MD, USA) was used to create two- and three-dimensional surface plot images from each ion density map.

Immunohistochemistry. Subsequent tissue sections from the imaged sample were cut (5 μm), placed on slides, and stored at –20˚C when necessary. For IHC sections were fixed for 10 min in 4˚C acetone, followed by thorough rinsing in Tris-buffered saline, pH 7.6 (TBS). Endogenous peroxide and non-specific background were blocked by applying a peroxidase blocking reagent (Dako Cat. #S2001) for 5 min followed by buffer rinse. The predetermined optimum dilution of each antibody was added to the appropriate slides and incubated at room temperature for 30 min (Ki-67, MIB1 clone, Dako Cat. #M7240, diluted 1:50; Calcyclin, CACY-100 clone, Sigma Cat. #S5049, diluted 1:10,000; and MIF, Santa Cruz Cat.#sc20121, diluted 1:100). Buffer washes and secondary reagents were applied following directions supplied by the manufacturer. For Ki-67 and MIF antibodies, these consisted of peroxidase conjugated secondary

reagents of the Dako LSAB2 system (Cat. #K0673). For the Calcyclin antibody, a peroxidase conjugated polymer was used (Dako Monoclonal EnVision+, Cat. #K4006). Specific antibody binding sites were localized by reaction with a 0.5% 3,3-diaminobenzidine-0.01% H_2O_2, and counterstained with hematoxylin. After alcohol and xylene dehydration, slides were coverslipped using a permanent mounting medium. Address for Sigma: St. Louis, Mo. 63103.

Protein identification. To identify *m/z* 18,931, *m/z* 21,069, and *m/z* 21,854, skeletal muscle (300 mg) from a different patient was suspended in homogenization buffer (0.25 mol/L sucrose, 10 mmol/L Tris, protease inhibitors (pH 7.6)), homogenized and further prepared for HPLC separation as described in (24). After separation, fractions containing the proteins of interest were further separated using 1-dimensional SDS on a 4-12% Bis Tris precast gel (Invitrogen) for 35 min at 200 V. All gels were fixed with 50% methanol, 10% acetic acid for 15 min and then stained with Colloidal Blue overnight followed by destaining with water. The bands representing the molecular weights of the *m/z* signals observed in the MALDI spectra were excised from the gel and equilibrated in ammonium bicarbonate buffer (0.4 mol/L, 25 μL) and reduced with DTT (5 μL, 45 mmol/L) for 15 min at 60˚C and alkylated with iodoacetimide (5 μL, 100 mmol/L) for 15 min at room temperature in the dark. Trypsin (0.05 μg) was added and the samples were digested for 24 hours at 37˚C. Peptides were extracted using 60% acetonitrile/ 40% H_2O/ 0.1% TFA (3x100 mL), pooled and dried. Samples were reconstituted in 0.1% TFA and desalted using a C18 ZipTiP (Millipore) according to the manufacturer's protocol and kept at 4˚C until further analysis. LC-MS/MS analyses were performed on a ThermoFinnigan LTQ linear ion trap mass spectrometer equipped with a ThermoFinnigan Surveyor quanterery HPLC pump and a microelectrospray source (Thermo Electron, San Jose, CA, USA). Reversed-phased separation of the tryptic peptides was performed using fused silica capillary tips (Polymicro Technologies, 100 μm i.d., 360 μm o.d.) packed with Monitor C18 (5 μm, Column Engineering). The HPLC pump was operated at a flow rate of 175 μL/min and was split to achieve a flow through the column of 700 nL – 1000 nL min^{-1}. Mobile phase A consisted of 0.1% formic acid and Mobile phase B consisted of 0.1% formic acid in acetonitrile. After equilibrating the column with 100% A, the peptides were eluted off the column with a gradient of 5% B for 5 min, increased to 50% B by 50 min, then increased to 80% by 52 min, increased to 90% by 55 min and held for 1 min. The gradient was then returned to 5% B over the next 5 min and continued at that composition until the end of the run at 71 min. LTQ ion trap mass spectrometer and HPLC solvent gradients were controlled by Xcalibur 1.4 software (Thermo Electron). MS/MS spectra were acquired using a data dependent scanning mode with one full MS scan (*m/z* 400-2000) followed by three MS/MS scans of the three most intense precursor masses at a 35% collision energy. Tandem mass spectra from LCMS/MS analyses were searched against the human database using SEQUEST (Thermo Electron, San Jose, CA, USA) and data filtered using a custom-designed software tool (Complete Heirarchical Integration of Protein Searches, CHIPS) (25) based upon the following filtering criteria: Cross correlation (Xcorr) value of >1.8 for doubly charged ions, and >2.5 for triply charged ions. A RSp (ranking of primary score) value of <5 and a Sp value (primary score) >350 were also required for positive peptide identifications that match to the intact protein. Identification of *m/z* 9,910, *m/z* 10,092, and *m/z* 11,385 have been described previously (24). Briefly, proteins were extracted from tumor tissue and HPLC separated as described above. HPLC fractions containing the *m/z* of interest were digested with trypsin, purified and concentrated with ZipTip reversedphase chromatography per the manufacturer's instructions (Millipore, Billerica, MA, USA). A sample aliquot (500 nl) was mixed on the target plate with α-cyano-4-hydroxycinnamic acid matrix (500 nl; prepared at 10 mg/mL in 50/50/0.1 (*v/v/v*) water/acetonitrile/TFA). The samples were allowed to dry and were analyzed with a 4700 Proteomics Analyzer MALDI TOF-TOF mass spectrometer (Applied Biosystems). Peptide mass fingerprinting was done in MS mode, and peptide masses were searched against the National Center for Biotechnology Information and SwissProt databases. Results were confirmed by sequencing the tryptic peptides in MS/MS mode and searching for the amino acid *m/z* values in the National Center for Biotechnology Information and SwissProt databases using a commercially available database searching algorithm (MASCOT).

Results

The optical image of a resected, human soft tissue sarcoma is shown in Figure 1A. Visual analysis shows the malignant fibrous histiocytoma adjacent to fibrovascular tissue and skeletal muscle, the specimen measuring 1.0x2.5 cm. A layer of fibrous stroma attached to the tumor and several small vessels within the skeletal muscle and fibrovascular tissue were present. Examination of the specimen after hematoxylin-eosin and cresyl violet staining indicated no cellular transformation or other abnormal phenotypes beyond the histological tumor margin. The mass spectrometric images, taken at a resolution of 250 μm, are shown in Figure 1B.

The mass spectra obtained from 3,000 spots in the array of the tissue revealed many *m/z* (mass-to-charge) species that are known to be present in certain tumors, including calcyclin (*m/z* 10,092) (26), calgranulin A (*m/z* 10,835) (27), calgizzarin (*m/z* 11,651) (26), and macrophage migration inhibitory factor (MIF, *m/z* 12,338) (28), as well as histone H4 (*m/z* 11,305) (29). An ion density image of each protein was generated in order to determine if these proteins traverse into the histologically normal tissue. As shown in Figure 1B, signal intensity, or relative concentration, of each protein varied markedly across the tumor. Interestingly, signals in discrete regions of the adjacent, histologically-normal tissue, oftentimes of comparable intensity of that found in the tumor, were also observed. It is important to note that these protein distribution patterns are not related to soft tissue type (*i.e.,* fibrovascular tissue *vs*. skeletal muscle), but to the proximity of the area to the tumor. However, some proteins were localized specifically to the tumor without detectable infiltration into the histologically normal tissue. While *m/z* 9,910, previously identified as acyl CoA-binding protein in breast tumors (24), is abundantly expressed within the tumor region, its expression was quite

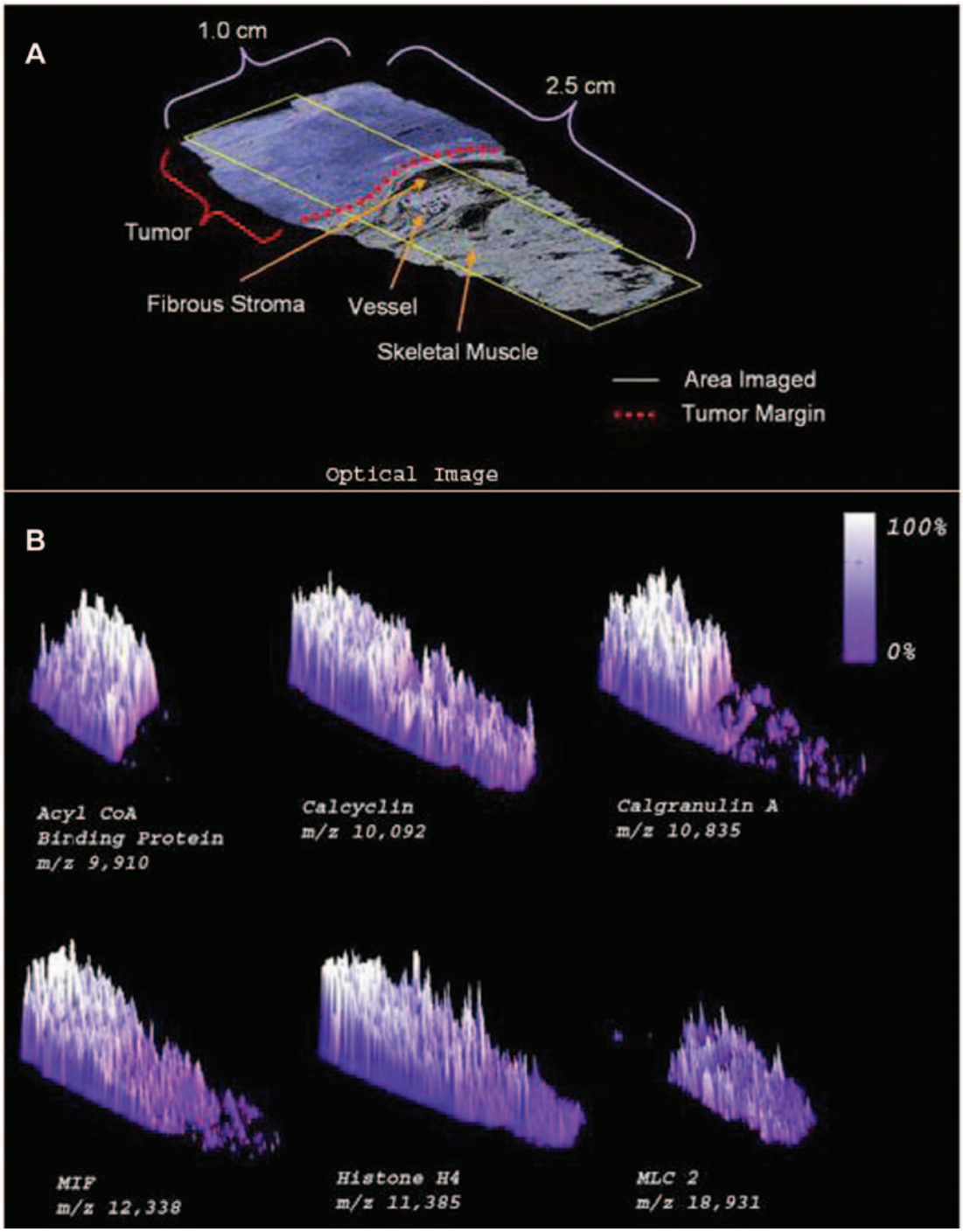

Figure 1. *A) Optical image of tissue section prior to MALDI imaging. After sectioning in a cryostat, the tissue sample was transferred to a MALDI-compatible glass slide and stained with cresyl violet for microscopic analysis. Specimen dimensions are 1.0x2.5 cm. The tumor is bordered by fibrovascular stroma and skeletal muscle. A clear tumor margin exists (red) with no visually distinguishable cancer morphology in the adjacent skeletal muscle. For IMS matrix droplets were discretely deposited with an acoustic microdispensing robot across the entire specimen as outlined (yellow) with a grid of 30x100 spots with 250 μm between spots. B) IMS characterizes protein localization from the tumor margin into histologically normal tissue. After spectra processing and baseline subtraction, signals consistent with previously identified proteins from were imaged into a 2-dimensional ion density map, including acyl-CoA binding protein (m/z 9,910), calcyclin (m/z 10,092), calgranulin A (m/z 10,835) MIF (m/z 12,338), histone H4 (m/z 11,385) and MLC2 (m/z 18,931). As described in the Methods section, images were recreated into 3-dimensional representations in X and Y coordinates of the tissue surface and intensity of the signal of interest. Deep purple is representative of low protein expression and white is representative of maximum protein expression relative to the most intense signal for the specific m/z in the tissue.*

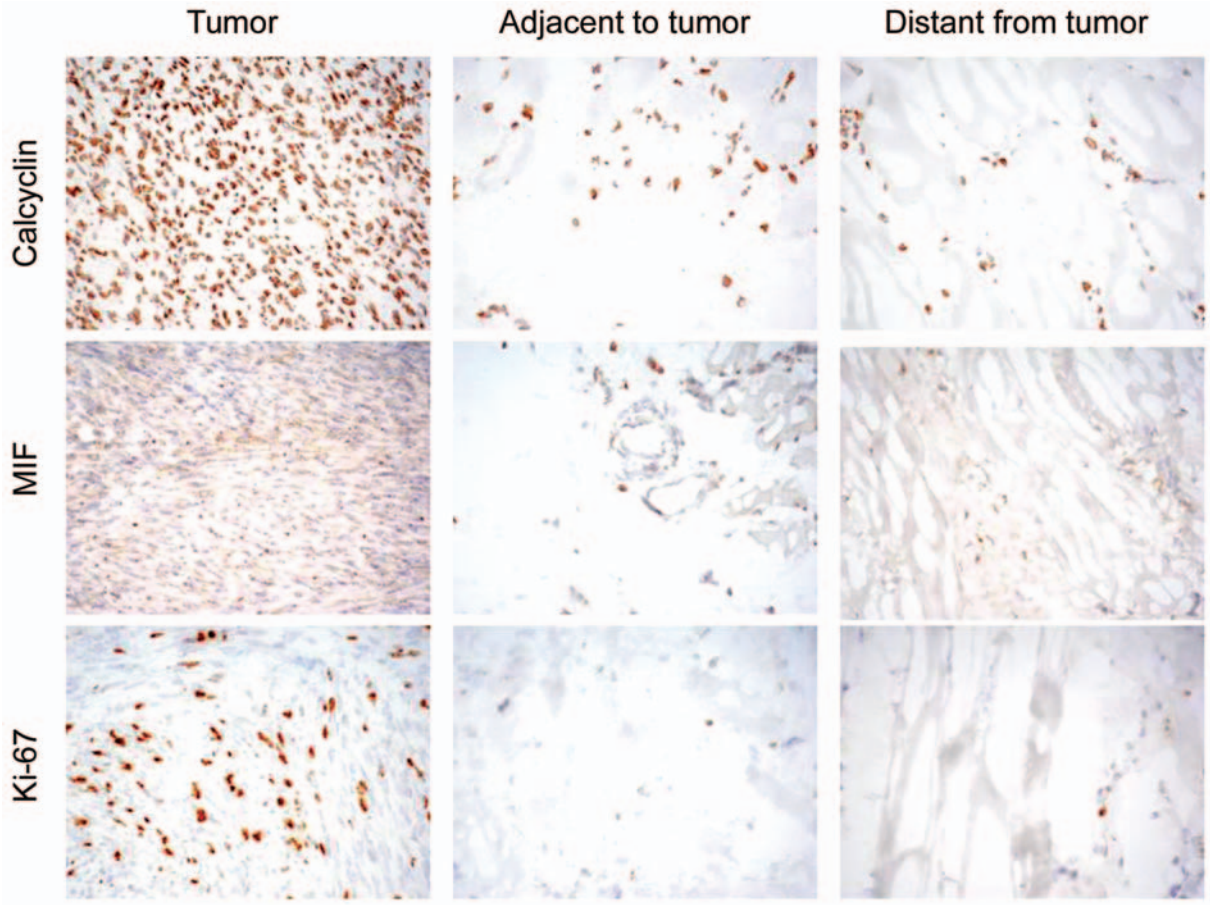

Figure 2. *Immunohistochemical staining of calcyclin, MIF and Ki-67. Representative areas from tumor/sarcoma, normal tissue adjacent to tumor, and normal tissue away from tumor are shown. Calcyclin and MIF immunostaining shows patchy moderate staining in the cytoplasm of tumor cells, while fewer cells in the adjacent normal soft tissue show positive staining. Cells most distant from the tumor show decreased positive staining. Ki-67 immunostaining shows strong positivity in numerous tumor cell nuclei, indicating a relatively high proliferation rate. Rare nuclear positivity is seen in normal adjacent soft tissue. Rare nuclear positivity is seen in soft tissue away from the tumor. All photographs were taken at 400x magnification.*

low beyond the histologically defined tumor margin. As expected, proteins known to be present in normal tissue were only detected in the non-tumor region of skeletal muscle. For example, myosin light chain type 2 (MLC2, *m*/*z* 18,931), was detected almost exclusively throughout the skeletal muscle. Other ECM proteins, including myosin light polypeptide-3 (*m*/*z* 21,854) and myosin light chain-1 (*m*/*z* 21,069), were exclusively localized in the non-tumor tissue (data not shown).

For purposes of validation, the distribution of a number of these proteins was confirmed using immunohistochemical staining on subsequent tissue sections (Figure 2). For example, immunostaining for calcyclin and MIF showed high expression in the tumor, as well as a gradient decrease beyond the tumor histological margin. Immunostaining for Ki-67, a cell proliferation marker, showed strong positivity in numerous tumor cell nuclei. Rare nuclear positivity was observed in normal adjacent soft tissue and in the skeletal muscle most distal from the tumor. Ki-67 expression level was consistent throughout the skeletal muscle (data not shown), indicating the absence of highly active proliferating cells beyond the histologic margin.

Molecular analysis of tumor microenvironment. The mass spectrometric data show significant molecular changes beyond the histologic tumor margin, well into the 'normal' tissue. To help define the extent of these molecular changes, the combined or summed molecular images of several proteins (calcyclin, calgranulin A and MIF) that are abundantly expressed in tumors, including high grade soft tissue sarcoma (30), are shown in Figure 3. The relative abundance of this combined signal decreased from the histologic margin but persisted far into normal tissue. This was also true for many, but not all, proteins, showing abnormal levels of expression

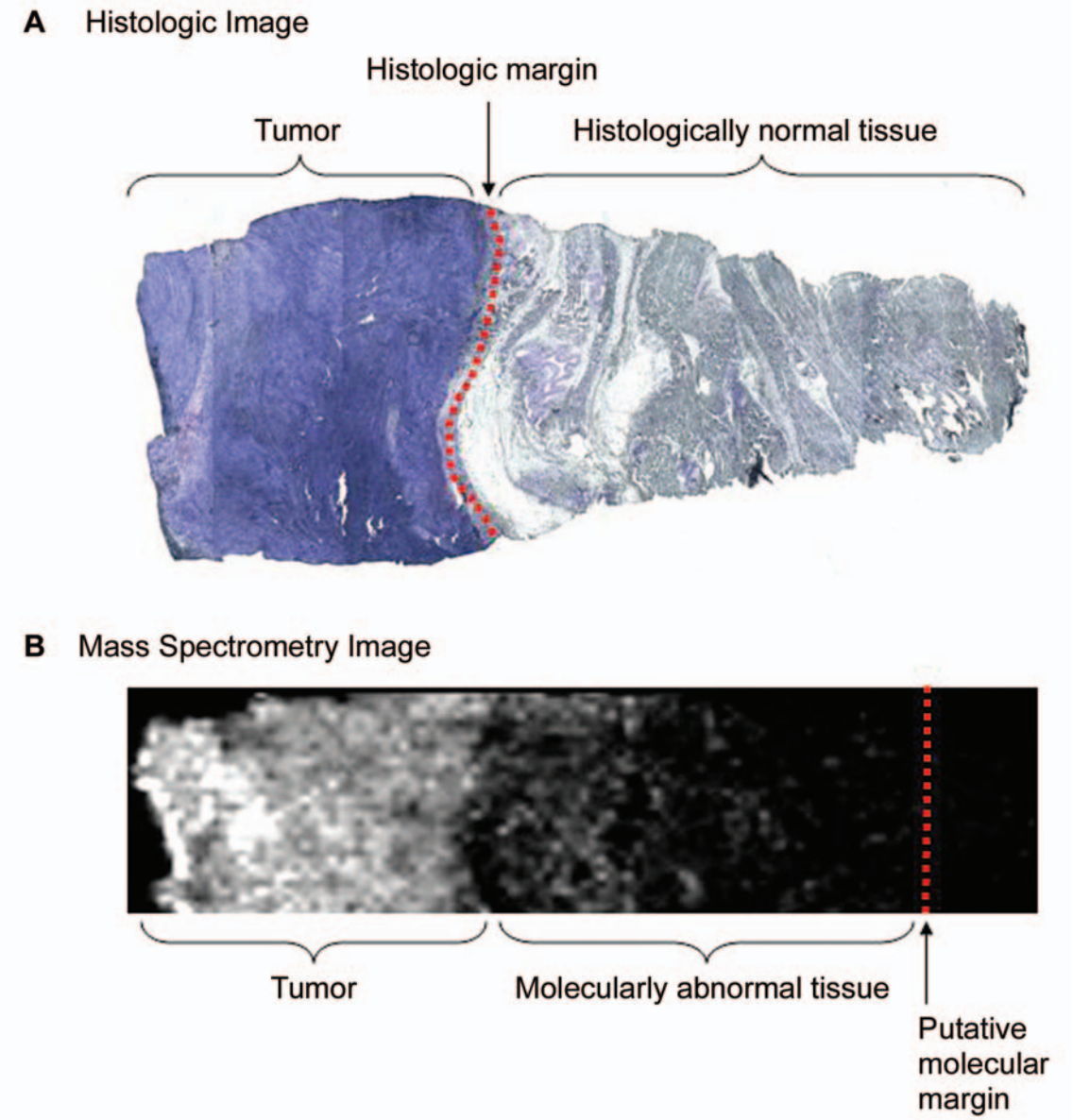

Figure 3. *A) The optical image of the cresyl violet stained specimen is shown. The tumor and histologically normal tissue determined by H&E staining are depicted. Red dots demonstrate the histologically-defined tumor margin. B) The molecular assessment of the tumor margin by IMS was created by combining signal intensities of calcyclin (m/z 10,092), calgranulin A (m/z 10,835) and MIF (m/z 12,338). Tumor and molecularly abnormal tissue regions are depicted. The putative molecular tumor margin is described by red dots.*

approximately 1.5 cm beyond the histologic margin. Although several specific proteins were chosen to graphically illustrate this phenomenon, many other proteins or combination of proteins may be used in such an assessment.

Discussion

This study utilized IMS to define the protein micro-environment adjacent to a tumor, and to detect proteins specific to tumor or non-tumor regions. Localization of protein markers downstream of the histologic tumor margin could represent regions of transformed cells, or transforming cells, that are morphologically indistinguishable from their genetically normal counterparts, yet maintain potential for tumor invasion and metastasis. Extratumoral expression of several cancer proteins in this study is reinforced by their putative involvement in neoplasia, cancer progression and metastasis.

Although the basis of this study focused on a soft tissue sarcoma specimen, a number of these proteins have been implicated in other cancers. For example, reports cite calcyclin dysregulation in pancreatic carcinoma (31) overexpression in invasive margins of colorectal adenocarcinomas, potentially leading to metastasis (32). Expression of calcyclin beyond the histological margin is consistent with its biological role in the phosphorylation inhibition of annexin, myosin heavy chain and p53 (33). The S100 family members, including calcyclin, as well as calgranulin, also interact with cytoskeletal elements, including microtubules and actin, leading to dysfunction in microtubule assembly and increased motility and invasion (34). Calgranulin isoforms A and B have been shown to exist in cystic fluid and sera from patients diagnosed with ovarian cancer (35). This study expands the role of calcyclin and calgranulin A to possible molecular markers that may be useful in defining surgical margins in soft tissue sarcomas.

Macrophage migration inhibitory factor (MIF) has been recently implicated in regulating tumor migration and expression of angiogenic factors in hepatocellular carcinoma (36), as well as in the regulation host inflammatory and immune responses. Under normal physiological conditions, MIF circulates at basal levels in serum and is also secreted as an immune response from activated monocytes and macrophages (37-39). Additionally, MIF has been linked to fundamental processes that control cell proliferation, differentiation, angiogenesis and tumor progression (40). In particular, one report shows that MIF inactivates the tumor suppressing activity of p53 (41), and overexpression of MIF has been recently observed in human melanoma (42), breast carcinoma (43), metastatic prostate cancer (44) and adenocarcinoma of the lung (45). Although the exact function of MIF in tumor progression remains unclear, studies have linked its expression to increased macrophage-derived angiogenesis (46). It has been suggested that increased MIF secretion by tumor cells may aid in tumor promotion, survival and metastasis by inducing release of angiogenic factors (47). Our imaging experiments, followed by immunohistochemical validation, show MIF expression highest in tumor and still abundant well beyond the histologic margin. Consistent with the aggressive phenotype of this particular sarcoma specimen, MIF expression beyond the tumor margin might be explained as a mechanism giving rise to tumor cell-mediated angiogenesis and promotion of tissue vasculature. Taken together, MIF expression, along with other proteins, such as calcyclin and calgranulin A, may represent clusters of tumor cells that appear non-pathologic under standard histological analysis, such as Ki-67.

The power of IMS resides in its molecular specificity and its ability to rapidly assess localization and relative abundance of proteins within an hour of less after specimen procurement. Most importantly, it is ideal for discovery in that it does not require knowledge of protein composition nor require reagents specific to the identification of one or more proteins. Ongoing studies include other tumor types and subtypes in an attempt to discover novel molecules that will define molecular tumor margins, and eventually aid in more effective surgical procedures.

Acknowledgements

The authors are grateful to Sandy Olson, M.S., for expert help in the immunohistochemistry studies. The authors thank Dale S. Cornett, Ph.D., and Pierre Chaurand, Ph.D., for their helpful suggestions and review of the manuscript. The authors also thank Hans-Rudolf Aerni for his expert assistance in sample preparation. Funding from NIH/NIGMS 5R01 GM 58008, 5R33 CA86243-03, the T.J. Martell Foundation, the Robert J. Kleberg Jr. and Helen C. Kleberg Foundation and the Vanderbilt-Ingram Comprehensive Cancer Center are also acknowledged.

References

1 Emrich LJ, Ruka W, Driscoll DL and Karakousis CP: The effect of local recurrence on survival time in adult high-grade soft tissue sarcomas. J Clin Epidemiol *42*: 105-110, 1989.

2 Stotter AT, A'Hern RP, Fisher C, Mott AF, Fallowfield ME and Westbury G: The influence of local recurrence of extremity soft tissue sarcoma on metastasis and survival. Cancer *65*: 1119-1129, 1990.

3 Masasyesva BG, Tong BC, Brock MV, Pilkington T, Goldenberg D, Sidransky D, Harden S, Westra WH and Califano J: Molecular margin analysis predicts local recurrence after sublobar resection of lung cancer. Int J Cancer *113*: 1022-1025, 2005.

4 Ohori M, Wheeler TM, Kattan MW, Goto Y and Scardino PT: Prognostic significance of positive surgical margins in radical prostatectomy specimens. J Urol *154*: 1818-1824, 1995.

5 Miller AR, Brandao G, Prihoda TJ, Hill C, Cruz AB Jr and Yeh IT: Positive margins following surgical resection of breast carcinoma: analysis of pathologic correlates. J Surg Oncol *86*: 134-140, 2004.

6 Landheer ML, Klinkenbijl JH, Pasker-de Jong PC and Wobbes T: Residual disease after excision of non-palpable breast tumours: analysis of tumour characteristics. Eur J Surg Oncol *30*: 824-828, 2004.

7 McKee MD, Liu DF, Brooks JJ, Gibbs JF, Driscoll DL and Kraybill WG: The prognostic significance of margin width for extremity and trunk sarcoma. J Surg Oncol *85*: 68-76, 2004.

8 Kawaguchi N, Ahmed AR, Matsumoto S, Manabe J and Matsushita Y: The concept of curative margin in surgery for bone and soft tissue sarcoma. Clin Orthop Relat Res *419*: 165-172, 2004.

9 Snyderman CH and D'Amico F: Outcome of carotid artery resection for neoplastic disease: a meta-analysis. Am J Otolaryngol *13*: 373-380, 1992.

10 Braakhuis BJ, Tabor MP, Kummer JA, Leemans CR and Brakenhoff RH: A genetic explanation of Slaughter's concept of field cancerization: evidence and clinical implications. Cancer Res *63*: 1727-1730, 2003.

11 Brennan JA, Mao L, Hruban RH, Boyle JO, Eby YJ, Koch WM, Goodman SN and Sidransky D: Molecular assessment of histopathological staging in squamous-cell carcinoma of the head and neck. N Engl J Med *332*: 429-435, 1995.

12 van Houten VM, Leemans CR, Kummer JA, Dijkstra J, Kuik DJ, van den Brekel MW, Snow GB and Brakenhoff RH: Molecular diagnosis of surgical margins and local recurrence in head and neck cancer patients: a prospective study. Clin Cancer Res *10*: 3614-3620, 2004.

13 Nathan CA, Amirghahari N, Abreo F, Rong X, Caldito G, Jones ML, Zhou H, Smith M, Kimberly D and Glass J: Overexpressed eIF4E is functionally active in surgical margins of head and neck cancer patients *via* activation of the Akt/mammalian target of rapamycin pathway. Clin Cancer Res *10*: 5820-5827, 2004.

14 Nathan CA, Amirghahri N, Rice C, Abreo FW, Shi R and Stucker FJ: Molecular analysis of surgical margins in head and neck squamous cell carcinoma patients. Laryngoscope *112*: 2129-2140, 2002.

15 Fradet V, Lessard L, Begin LR, Karakiewicz P, Masson AM and Saad F: Nuclear factor-kappaB nuclear localization is predictive of biochemical recurrence in patients with positive margin prostate cancer. Clin Cancer Res *10*: 8460-8464, 2004.

16 Ananthanarayanan V, Deaton RJ, Yang XJ, Pins MR and Gann PH: Alphamethylacyl-CoA racemase (AMACR) expression in normal prostatic glands and high-grade prostatic intraepithelial neoplasia (HGPIN): association with diagnosis of prostate cancer. Prostate *63(4)*: 341-346, 2004.

17 Merrick DT, Haney J, Petrunich S, Sugita M, Miller YE, Keith RL, Kennedy TC and Franklin WA: Overexpression of vascular endothelial growth factor and its receptors in bronchial dypslasia demonstrated by quantitative RT-PCR analysis. Lung Cancer *48*: 31-45, 2005.

18 Stoeckli M, Chaurand P, Hallahan DE and Caprioli RM: Imaging mass spectrometry: a new technology for the analysis of protein expression in mammalian tissues. Nat Med *7*: 493-496, 2001.

19 Chaurand P, Schwartz S, Reyzer M and Caprioli R: Imaging mass spectrometry: principles and potentials. Toxicol Pathol *33*: 92-101, 2005.

20 Caldwell RL and Caprioli RM: Tissue profiling by mass spectrometry: a review of methodology and applications. Mol Cell Proteomics *4*: 394-401, 2005.

21 Stoeckli M, Staab D, Staufenbiel M, Wiederhold KH and Signor L: Molecular imaging of amyloid beta peptides in mouse brain sections using mass spectrometry. Anal Biochem *311*: 33-39, 2002.

22 Aerni H-R. C, D. S and Caprioli RM: Automated acoustic matrix deposition for MALDI sample preparation. Anal Chem *78(3)*: 827-834, 2005.

23 Chaurand P, Schwartz SA, Billheimer D, Xu BJ, Crecelius A and Caprioli RM: Integrating histology and imaging mass spectrometry. Anal Chem *76*: 1145-1155, 2004.

24 Reyzer ML, Caldwell RL, Dugger TC, Forbes JT, Ritter CA, Guix M, Arteaga CL and Caprioli RM: Early changes in protein expression detected by mass spectrometry predict tumor response to molecular therapeutics. Cancer Res *64*: 9093-9100, 2004.

25 Ham A-J, Jones JA and Liebler DC: CHIPS (Complete Hierarchical Integration of Protein Searches), a database program for storing, filtering and comparing Sequest outputs. Asms Conference Proceedings, Nashville, TN, USA, 2004.

26 Schwartz SA: Proteomic-based classification of human brain tumors by mass spectrometry. Edited by Nashville, Vanderbilt University, p. 139, 2004.

27 Chaurand P, Sanders ME, Jensen RA and Caprioli RM: Proteomics in diagnostic pathology: profiling and imaging proteins directly in tissue sections. Am J Pathol *165*: 1057-1068, 2004.

28 Campa MJ, Wang MZ, Howard B, Fitzgerald MC and Patz EF Jr: Protein expression profiling identifies macrophage migration inhibitory factor and cyclophilin a as potential molecular targets in non-small cell lung cancer. Cancer Res *63*: 1652-1656, 2003.

29 Reyzer ML, Hsieh Y, Ng K, Korfmacher WA and Caprioli RM: Direct analysis of drug candidates in tissue by matrix-assisted laser desorption/ionization mass spectrometry. J Mass Spectrom *38*: 1081-1092, 2003.

30 Caldwell RL, Holt GE and Caprioli RM: Tissue profiling by MALDI mass spectrometry distinguishes clinical grades of soft tissue sarcomas. Cancer Gemomics and Proteomics *2*: 333-346, 2005.

31 Crnogorac-Jurcevic T, Missiaglia E, Blaveri E, Gangeswaran R, Jones M, Terris B, Costello E, Neoptolemos JP and Lemoine NR: Molecular alterations in pancreatic carcinoma: expression profiling shows that dysregulated expression of S100 genes is highly prevalent. J Pathol *201*: 63-74, 2003.

32 Komatsu K, Murata K, Kameyama M, Ayaki M, Mukai M, Ishiguro S, Miyoshi J, Tatsuta M, Inoue M and Nakamura H: Expression of S100A6 and S100A4 in matched samples of human colorectal mucosa, primary colorectal adenocarcinomas and liver metastases. Oncology *63*: 192-200, 2002.

33 Schafer BW, Wicki R, Engelkamp D, Mattei MG and Heizmann CW: Isolation of a YAC clone covering a cluster of nine S100 genes on human chromosome 1q21: rationale for a new nomenclature of the S100 calcium-binding protein family. Genomics *25*: 638-643, 1995.

34 Donato R: S100: a multigenic family of calcium-modulated proteins of the EFhand type with intracellular and extracellular functional roles. Int J Biochem Cell Biol *33*: 637-668, 2001.

35 Ott HW, Lindner H, Sarg B, Mueller-Holzner E, Abendstein B, Bergant A, Fessler S, Schwaerzler P, Zeimet A, Marth C and Illmensee K: Calgranulins in cystic fluid and serum from patients with ovarian carcinomas. Cancer Res *63*: 7507-7514, 2003.

36 Ren Y, Tsui HT, Poon RT, Ng IO, Li Z, Chen Y, Jiang G, Lau C, Yu WC, Bacher M and Fan ST: Macrophage migration inhibitory factor: roles in regulating tumor cell migration and expression of angiogenic factors in hepatocellular carcinoma. Int J Cancer *107*: 22-29, 2003.

37 Bernhagen J, Calandra T, Mitchell RA, Martin SB, Tracey KJ, Voelter W, Manogue KR, Cerami A and Bucala R: MIF is a pituitary-derived cytokine that potentiates lethal endotoxaemia. Nature *365*: 756-759, 1993.

38 Calandra T, Bernhagen J, Mitchell RA and Bucala R: The macrophage is an important and previously unrecognized source of macrophage migration inhibitory factor. J Exp Med *179*: 1895-1902, 1994.

39 Calandra T, Bernhagen J, Metz CN, Spiegel LA, Bacher M, Donnelly T, Cerami A and Bucala R: MIF as a glucocorticoid-induced modulator of cytokine production. Nature *377*: 68-71, 1995.
40 Mitchell RA and Bucala R: Tumor growth-promoting properties of macrophage migration inhibitory factor (MIF). Semin Cancer Biol *10*: 359-366, 2000.
41 Hudson JD, Shoaibi MA, Maestro R, Carnero A, Hannon GJ and Beach DH: A proinflammatory cytokine inhibits p53 tumor suppressor activity. J Exp Med *190*: 1375-1382, 1999.
42 Shimizu T, Abe R, Nakamura H, Ohkawara A, Suzuki M and Nishihira J: High expression of macrophage migration inhibitory factor in human melanoma cells and its role in tumor cell growth and angiogenesis. Biochem Biophys Res Commun *264*: 751-758, 1999.
43 Bini L, Magi B, Marzocchi B, Arcuri F, Tripodi S, Cintorino M, Sanchez JC, Frutiger S, Hughes G, Pallini V, Hochstrasser DF and Tosi P: Protein expression profiles in human breast ductal carcinoma and histologically normal tissue. Electrophoresis *18*: 2832-2841, 1997.
44 Meyer-Siegler K and Hudson PB: Enhanced expression of macrophage migration inhibitory factor in prostatic adenocarcinoma metastases. Urology *48*: 448-452, 1996.
45 Kamimura A, Kamachi M, Nishihira J, Ogura S, Isobe H, Dosaka-Akita H, Ogata A, Shindoh M, Ohbuchi T and Kawakami Y: Intracellular distribution of macrophage migration inhibitory factor predicts the prognosis of patients with adenocarcinoma of the lung. Cancer *89*: 334-341, 2000.
46 White ES, Strom SR, Wys NL and Arenberg DA: Non-small cell lung cancer cells induce monocytes to increase expression of angiogenic activity. J Immunol *166*: 7549-7555, 2001.
47 Meyer-Siegler KL, Bellino MA and Tannenbaum M: Macrophage migration inhibitory factor evaluation compared with prostate specific antigen as a biomarker in patients with prostate carcinoma. Cancer *94*: 1449-1456, 2002.

Received August 8, 2006
Accepted August 24, 2006